





Study on guardrail post behavior located on organic soil using simplified experimental and numerical methods

Hamid Reza Manaviparast^{1#} , Nuno Araújo¹ , Nuno Cristelo² ,
Tiago Miranda¹ 

Article

Keywords

Guardrail post
Road safety
Organic soil
Static loading
Dynamic loading

Abstract

For the purpose of road safety, it is vital to reduce the severity of road accidents and increase safety around the roadway area by deploying guardrails. In case of a car crash, a guardrail post must be deformable so that such restraint is not too abrupt due to the occupant's sensitivity. Soil type influences on the guardrail post behavior have been a somewhat unfounded variable due to the high soil heterogeneity and challenging interpretation of its real implications on the safety of guardrail systems. Since little attention is concentrated on evaluating the guardrail post behavior through simplified procedures, this article aims to provide a simplified experimental and numerical approach to study the behavior of guardrail posts located on organic soil. Results of laboratory and in-situ tests indicated that guardrail posts behavior located on organic soil depends on section orientation, driving depth, and loading speed. To confirm and compare the in-situ tests, simplified numerical simulations through Plaxis 3D software were carried out, and data from numerical modeling approved the accuracy of in-situ results.

1. Introduction

Infrastructures are always considered vital physical systems of a region or even a nation. These systems are primarily high-cost investments and are crucial to the prosperity and economy of a country. As an example of infrastructures, road infrastructure plays an essential role in the economy by helping to transport goods and services. It also plays a vital role in every community by keeping people connected to other regions and making it simple to commute to different regions.

Since road infrastructures have always played an essential role in developing civilizations, there was a need to create safe infrastructures. Road transport is a crucial aspect of today's society, in which the mobility of people and goods and traffic accidents resulting from this mobility has to be considered (Cui, 2020; Neves et al., 2018). The utilization of engineering treatments to enhance traffic safety is relevant to road safety design, and guardrails are one of the most widely used passive safety devices for roads (Mikusova, 2017). Guardrails, including W-beam, are labeled as weak or strong posts that adequately absorb a vehicle's impact to reduce the severity of vehicle crashes (Li et al., 2018; Gutowski et al., 2017). Worldwide, most guardrails are made of steel or concrete. Concrete barriers usually do not

include a foundation directly placed on the road surface. Hence, soil-barrier interaction for concrete barriers is not an issue. However, steel guardrail posts are usually bolted to a concrete deck or driven into the soil (Örnek et al., 2019). For the sake of soil influences on steel guardrails, the soil properties such as soil density, friction angle, and also post embedment depth become essential parameters affecting the guardrail behavior and performance (Örnek et al., 2019; Atahan et al., 2019; Sassi, 2011). With a lack of interaction between soil and adjacent structures, the steel guardrail cannot play a role as intended and cannot provide adequate safety for the impacting vehicles. Few studies have been done to evaluate the behavior of guardrail posts based on experimental analyses, but assessing the behavior of guardrail post located on organic soil through a simplified approach is scarce and needs more consideration to shed light on. Since the crash-test standards do not contain details of the soil properties, meaning that the guardrail post is embedded regardless of considering the in-situ soil condition (Ozcanan & Atahan, 2020; Yun et al., 2018), simplified in-situ tests were carried out to fully consider the effects of organic soil located beneath the guardrail post.

Pajouh et al. (2018) and Rohde et al. (1996) stressed that the guardrail post performance primarily depends on the interaction between the post and the surrounding soil.

[#]Corresponding author. E-mail address: id8028@alunos.uminho.pt

¹University of Minho, Department of Civil Engineering, Guimarães, Portugal.

²University of Trás-os-Montes e Alto Douro, School of Science and Technology, Vila Real, Portugal.

Submitted on November 27, 2021; Final Acceptance on March 23, 2022; Discussion open until August 31, 2022.

<https://doi.org/10.28927/SR.2022.077921>



This is an Open Access article distributed under the terms of the Creative Commons Attribution License, which permits unrestricted use, distribution, and reproduction in any medium, provided the original work is properly cited.

Tomlinson & Woodward (2007) revealed that in a guardrail post under a horizontal loading, driven into poor quality soil, a considerable part of the applied load was transferred to the post base and some of it to the surrounding soil. Gutowski et al. (2017) and Sassi (2011) revealed that the guardrail post tends to rotate alongside the imposed loading, soil blisters in the surrounding area, and the guardrail post compresses the soil in the front, causing it to fail. They also stated that the post might break at the pavement level in the dense soil, where the bending moment is maximum. Patzner et al. (1999) found that the guardrail post deflection tends to increase in soils with lower specific weight and decrease when the soil specific gravity increases. Based on Lim (2009) and Jeyapalan et al. (1984), steel guardrail post without the presence of concrete foundation indicates proper structural behavior during static and dynamic tests. Consequently, based on their investigations, it was decided not to consider the foundation effects on guardrail post performance as a simplified approach during this study.

To evaluate the performance of a guardrail post as a roadside safety device, as a common method, destructive full-scale crash testing is employed by engineers to assess the effects of impact on a guardrail post through a bogie vehicle. The extracted results serve to understand the dynamic and static behavior of the guardrail post. However, these tests are costly and need an extensive setup, instrumentation, and test vehicle wrecking. Consequently, this study decided to use a simplified approach instead of a costly setup as an advantageous option. Several simplified in-situ tests were conducted as experimental studies to provide results helping to evaluate the behavior of guardrail posts located on organic soil. For the purpose of more accuracy in the evaluation process of the guardrail post, several numerical models were analyzed using Plaxis 3D software as a numerical study to compare them with in-situ results.

2. Materials and methods

Finding and determining proper material properties are helpful to predict the material behavior better by engineers.

For this purpose, this study decided to study organic soil beneath the guardrail post, representing the adjacent soils found on the carriageways of ancient municipal roads in Portugal, the city of Guimarães. The selected test site belonged to the municipality of Guimarães. As a first step, there was a need to estimate the geotechnical parameters accurately. Hence, a set of tests was performed to determine the water content, organic matter content, particle size, consistency limits, and solid particle density. Triaxial and suction tests were also performed in the Civil Engineering Laboratory of the University of Minho.

For the post (Figure 1), the elastic and plastic deformability limits and the yield stress were analyzed in Civil and Mechanical Engineering laboratories at the University of Minho. The geometry of the guardrail post is the most typical type used in Portuguese municipal roads.

2.1 Soil characterization

Soil characterization is a necessary part of determining various geotechnical parameters of the soil. This process is vital to evaluate the fundamental parameters and determine other required geotechnical factors utilized during the execution of every geotechnical project. Regarding the fundamental geotechnical tests, the grain distribution curve (Figure 2) was obtained according to LNEC (1966). About other geotechnical parameters, it comprises 7% clay, 26% silt, and 67% of sand and gravel. The liquid (51%) and plastic (NP) Atterberg limits were obtained according to IGPAI (1969). The density of the solid particles was 2.5 (IGPAI, 1965), with an organic matter content of 6.1% (LNEC, 1967). Several undisturbed specimens (Figure 3) were collected in-situ, for the laboratory tests, with average volumetric weights of 15.3 kN/m³ (natural) and 12.3 kN/m³ (dry) and water contents between 17% and 29%.

A suction test, using the filter paper method (ASTM, 1994), was performed to obtain the retention curve by adjusting the van Genuchten model. Nine undisturbed specimens were collected, oven-dried at 110°C for 24 hours,

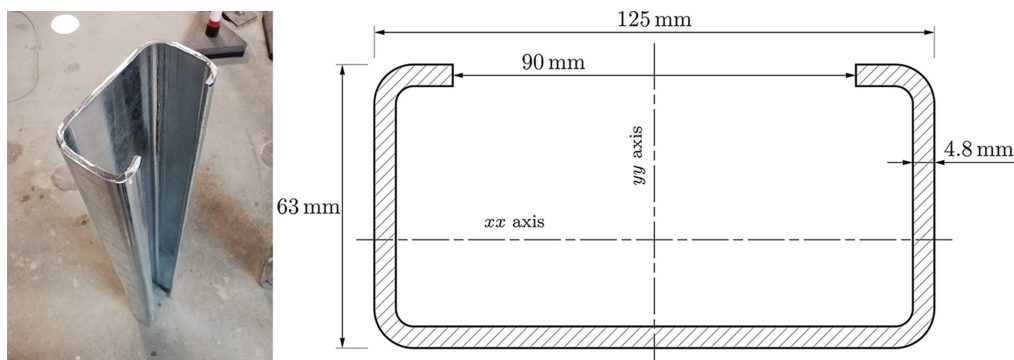


Figure 1. Geometry of the post used in the study.

Note: The axis *xx* and *yy* are defined.

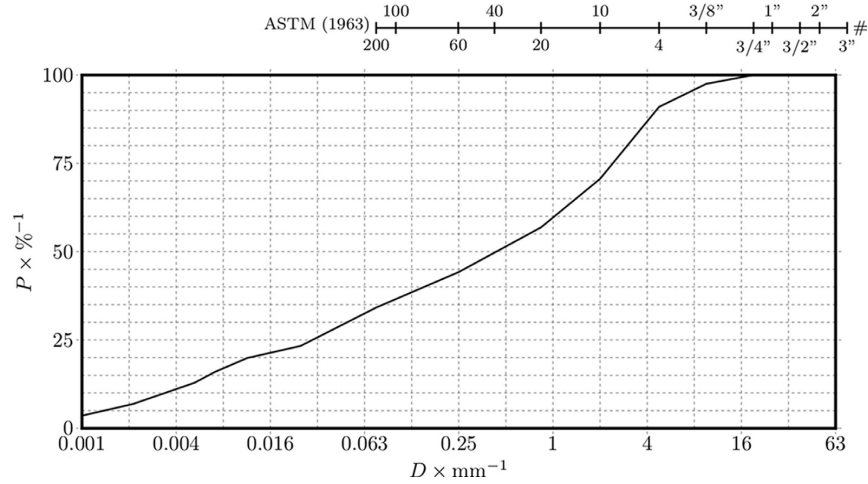


Figure 2. Particle size distribution of the soil (ASTM, 1963).



Figure 3. Extraction of undisturbed in-situ specimens.

and 3 filter papers (and water) were added and applied to each specimen so that the water content ranged from near zero to near saturated. One of the specimens was not used because it lost its integrity during assembly. The van Genuchten model (Equation 1) was used due to its high capacity for adjustment and convergence, in which ω_s is the saturated water content (in the study soil around 40%). The model has four parameters: ω_r (residual water content), α , n , and m . After adjustment to the experimental curve (Figure 4), $\omega_r = 3\%$, $\alpha = 0.15 \text{ kPa}^{-1}$, $n = 0.62$, and $m = 0.71$. The R -squared (R^2) of the fitting curve is equal to 0.985.

$$\omega = \omega_r \frac{\omega_s + \omega_r}{[1 + (\alpha \psi)^n]^m} \quad (1)$$

The results presented in Figure 5 to Figure 7 were obtained from triaxial tests on specimens extracted at a depth of 50 cm, according to BSI (1990). Figure 5 refers to a consolidation test

in which the pore pressure was maintained constant, and the confining pressure increased at a rate of 7 kPa/h from 1010 kPa to 1500 kPa, then reduced to 1010 kPa and finally raised to 1700 kPa while the backpressure was always 1000 kPa. During the test procedure in Figure 6 and Figure 7, the test speed was equal to $84 \cdot 10^{-6} \text{ mm/s}$. Figure 5 represents the specific volume v , the normal compression line (Equation 2) – obtained from the adjustment of the experimental results in the range $p' = [200 \text{ to } 700] \text{ kPa}$ – and the critical state line (Equation 3). The resulting strength parameters were $c' = 0 \text{ kPa}$, $\phi' = 34^\circ$, $c_u = 45 \text{ kPa}$, $\phi_u = 12^\circ$ (under saturated conditions), and $E = 3.8 \text{ MPa}$.

$$v(\text{NCL}) = \Gamma_{ICL} - \lambda_{NCL} \log_{10} \frac{p'}{1 \text{ kPa}} = 2.263 - 0.241 \log_{10} \frac{p'}{1 \text{ kPa}} \quad (2)$$

$$v(\text{CSL}) = \Gamma_{CSL} - \lambda_{CSL} \log_{10} \frac{p'}{1 \text{ kPa}} = 2.186 - 0.241 \log_{10} \frac{p'}{1 \text{ kPa}} \quad (3)$$

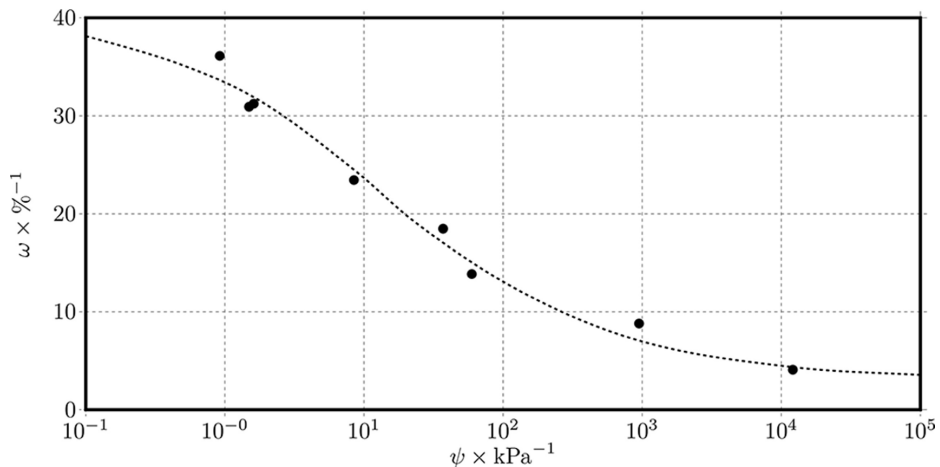


Figure 4. Wet soil retention curve (results and van Genuchten (1980) model adjustment).

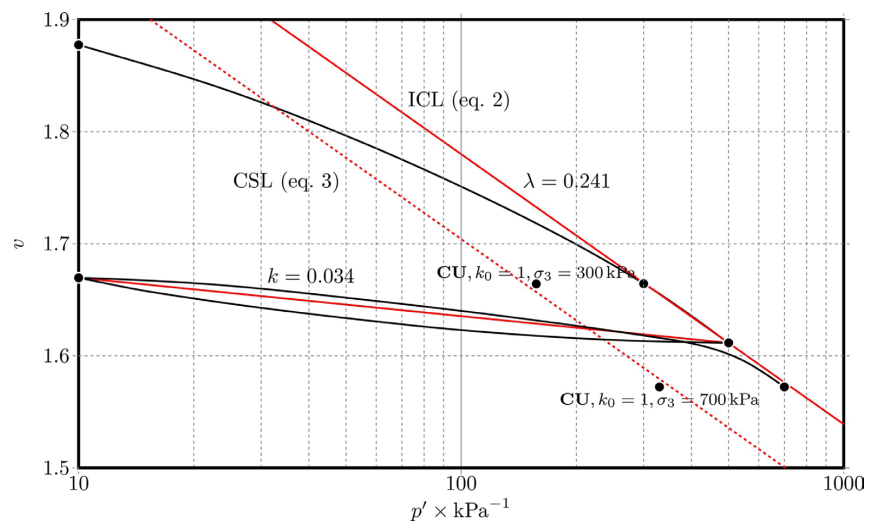


Figure 5. Triaxial tests results in the space $v = f(p')$.

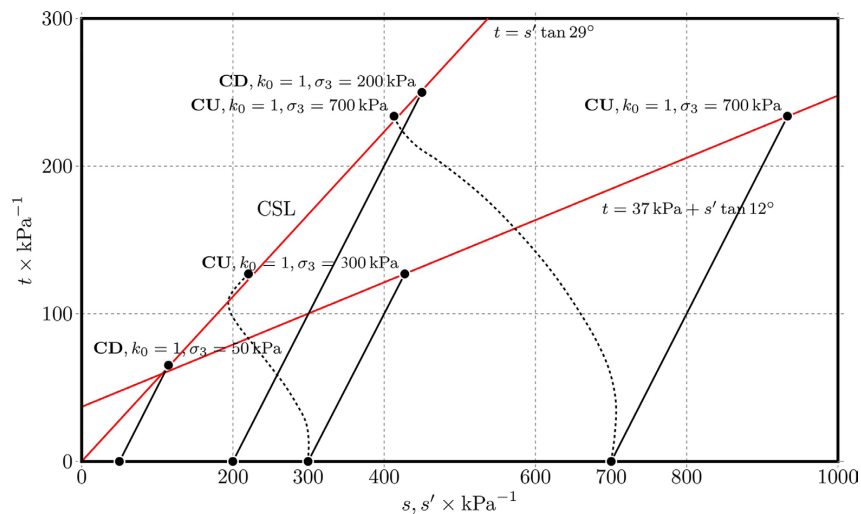


Figure 6. Triaxial tests results in the space $t = f(s \text{ or } s')$.

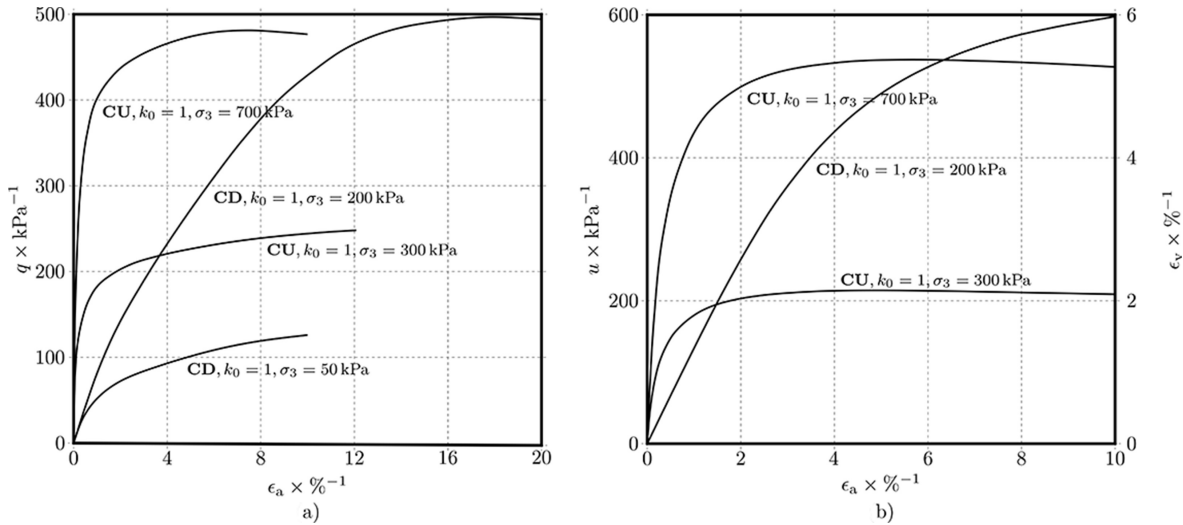


Figure 7. Triaxial tests results in the space a) $q = f(\epsilon_a)$; b) $(u \text{ or } \epsilon_v) = f(\epsilon_a)$.

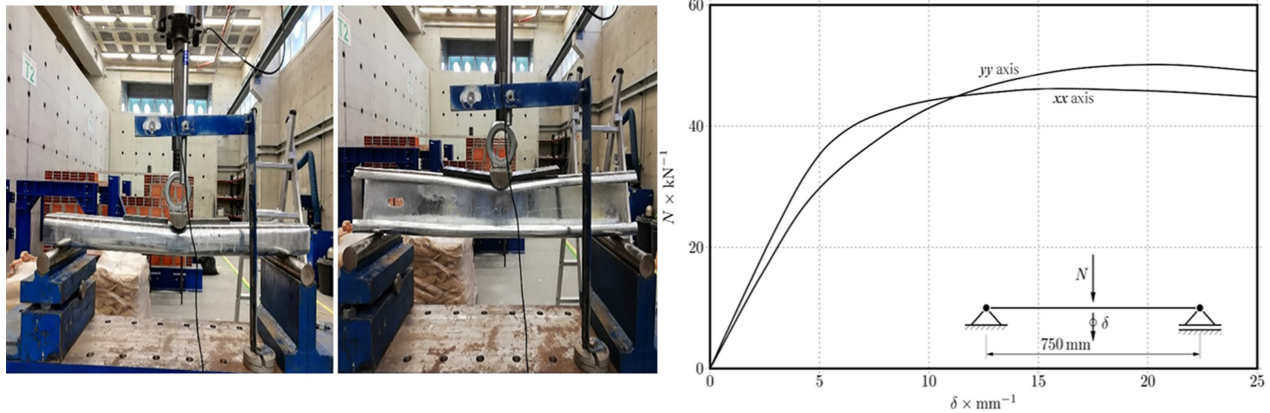


Figure 8. 3-point loading flexural test.

2.2 Post characterization

After performing the process of determining different geotechnical parameters of the soil, the guardrail post material was determined to start the evaluation of the guardrail post behavior under loading. The cold-formed metallic element (made from S235JR steel) forming the guardrail post has a C-shaped cross-section, with density $\rho = 7.86 \text{ Mg/m}^3$, Young modulus $E = 210 \text{ GPa}$, Poisson ratio $\nu = 0.3$ and yield stress $F_y = 235 \text{ MPa}$. It was acquired with two distinct lengths – 1.2 m or 1.7 m. It was loaded according to both moments of inertia using a hydraulic actuator (Figure 8). From the interpreted results, it was clear that it is not relevant which axis is loaded, as both responses are very similar.

3. Experimental results

An experimental test as the main component of each scientific study involves manipulating various factors in a

system to observe how that affects the final results. It is also helpful to offer a realistic prediction for real-world systems to be utilized by scientists and engineers. In order to assess road safety and evaluate the behavior of the guardrail post against static and dynamic loading, this study aimed to perform a proper characterization of the system through an experimental campaign comprising 8 posts. The main target of the campaign was changing (a) loading directions, (b) post depths, and (c) load speed (i.e., in static and dynamic conditions). All tests were carried out according to the conditions and water content found in situ, meaning that after the driving phase, no further compaction procedure was carried out on the surrounding soil. The guardrail posts were fully instrumented to indicate their real behavior during static and dynamic loading. In addition, in-situ geotechnical characterization of the soil profile was developed to define its geotechnical parameters better. It is noteworthy that all tests were performed with in-situ water content between 17% and 29%.

3.1 Geotechnical investigation

Geotechnical investigation is an operation in which engineers evaluate the geotechnical parameters of every project site to determine if the site is appropriate for the proposed purpose. The primary goal of each geotechnical investigation during every project is to investigate the soil conditions through performing various tests to provide accurate data for geotechnical engineers. Three different tests were performed in-situ: (a) dynamic penetrometer, (b) Marchetti dilatometer, and (c) plate load test (adapted for horizontal loading). The dynamic penetrometer test (Figure 9) was performed according to ISO (2005) through four drill holes to assure foundation homogeneity and confirm that the organic soil was present in the vicinity and along the entire length of the post. The Marchetti dilatometer test was carried out according to ISO (2017), mainly to obtain the coefficient of thrust at rest K_0 of the soil base. Nevertheless, it also allowed the estimation of the friction angle (ϕ) and the over-consolidation ratio (OCR). Surface results (i.e., up to about half a meter) were disregarded due to the influence of vegetation, desiccation, and low applied vertical stress σ_v . Since vertical stress is near zero up to about half a meter, it induces discrepancy when estimating the parameters. The obtained data interpretation made it possible to define $K_0 = 1.1$, OCR = 7, and $\phi = 39^\circ$ (in unsaturated conditions).

During the plate load test, it was decided to adopt the conventional test, which defines a vertical loading to a horizontal compression of the soil, thus mobilizing its passive earth pressure limit. The guardrail post movement depicts the evolution from the resting state to the passive limit state. It was performed by keeping the effective vertical stress constant while increasing the effective horizontal stress.

To perform the test, a hole was initially dug in the ground (Figure 10) with a length of 55 cm, a width of 37 cm, and a depth of 60 cm. By using a hydraulic jack, two plates with 30 cm in diameter were spread away at an average rate of 3 cm/min—two loading cycles were applied (Figure 11). For the 1st cycle, the plates were displaced until they were spread by 15 cm. Since the movement is symmetrical, an average individual displacement of 7.5 cm of each plate was reached. A 2nd cycle was then applied, after unloading, until failure was detected. Figure 10 shows that such point was reached when the soil horizontal compression was 330 kPa, as concluded from the cracks on the soil surface.

3.2 Post testing

Eight posts were deployed to assess and evaluate the behavior of the guardrail post through using test variables: (a) the two axes of inertia, (b) two post lengths, and (c) several imposed horizontal displacements (designed as *static test*) or forces (designed as *dynamic test*). To do so, it was required to define two testing procedures and instrumentation setup.

Regarding instrumentation, the guardrail post was instrumented with two load cells (Figure 12a) with the range of 0.50 kN to acquire the horizontal stress σ_h evolution during loading, which was calculated from the applied force, divided by the section of the dish (3 cm diameter) placed on each load cell. Two dishes were set at 15 cm and 30 cm below the surface to obtain the most significant stress associated with the passive thrust applied by the soil. Two accelerometers with the maximum admissible acceleration of 55g were also added to be used only on the dynamic tests, one at the surface (Figure 12b) and the other leveled with the horizontal loading force. Furthermore, five potentiometers with variable

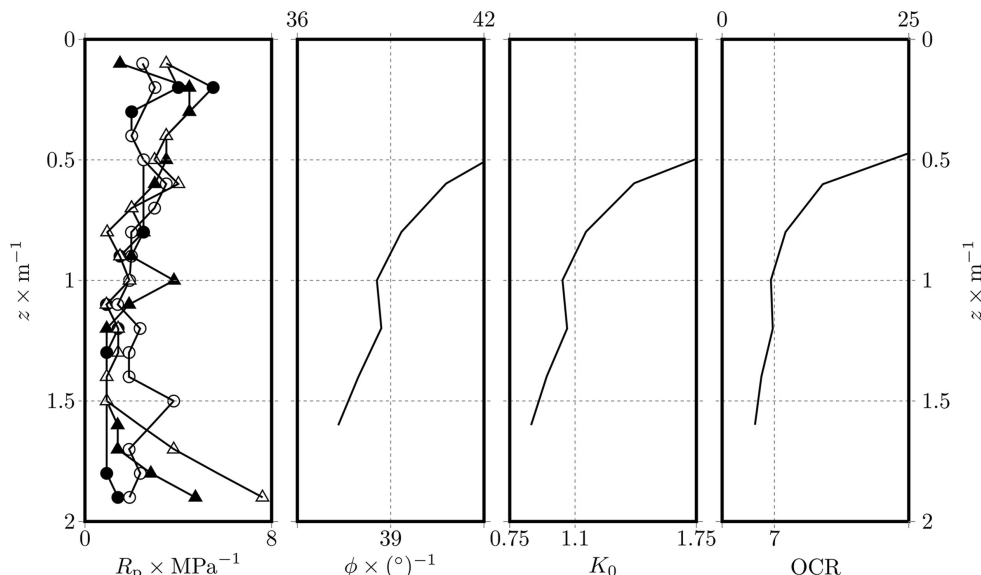


Figure 9. Geotechnical survey results (penetrometer and dilatometer).

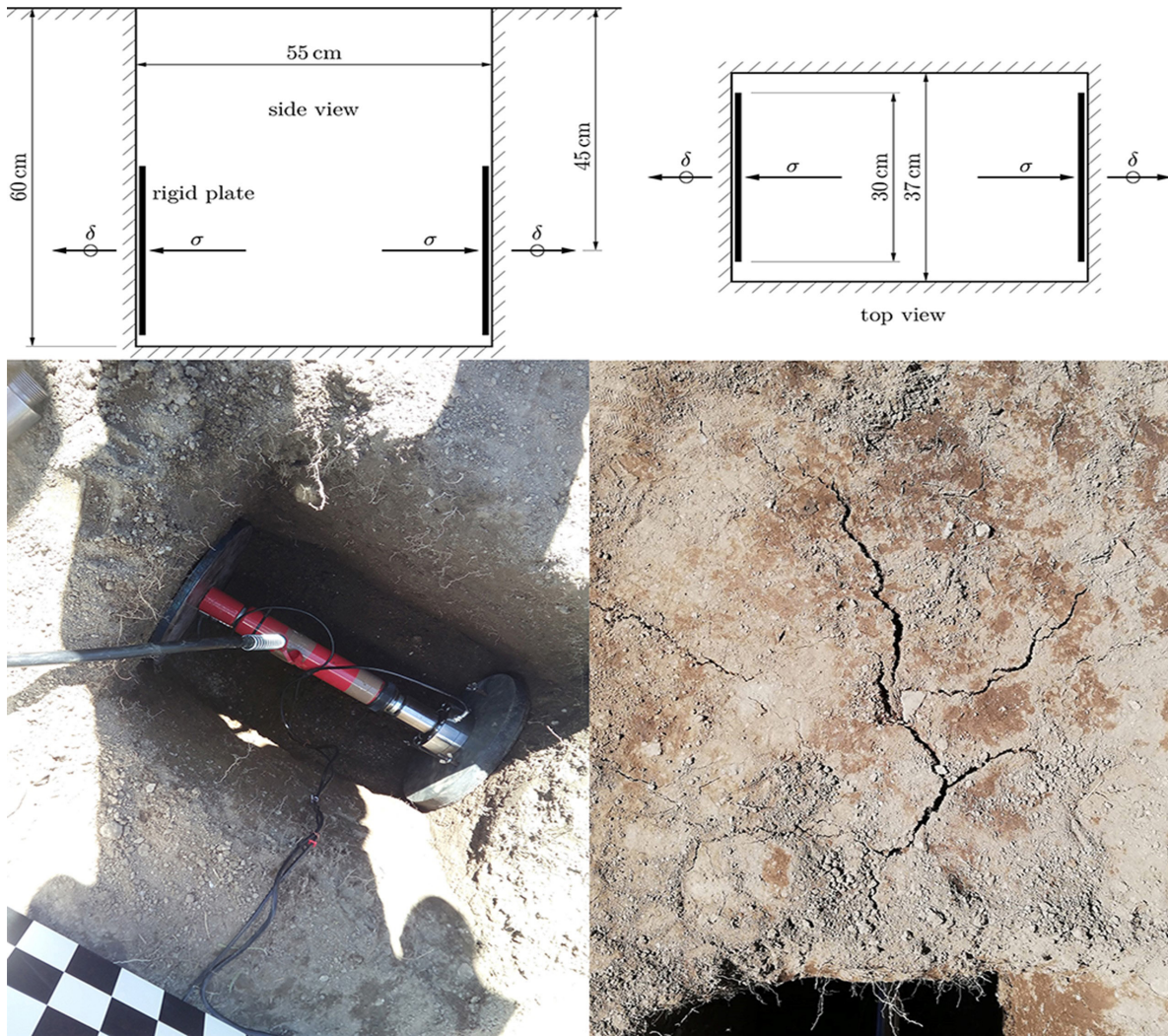


Figure 10. Horizontal load plate test geometry, assembly, and induced cracks.

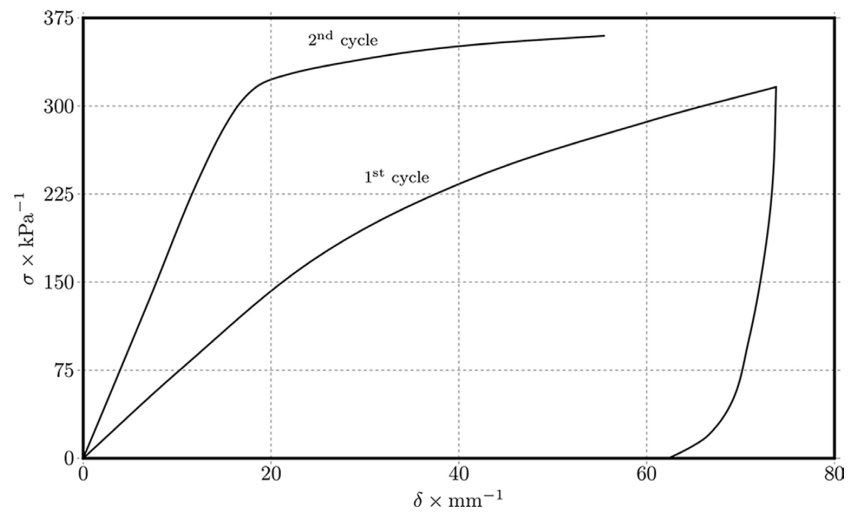


Figure 11. Horizontal load plate test results.

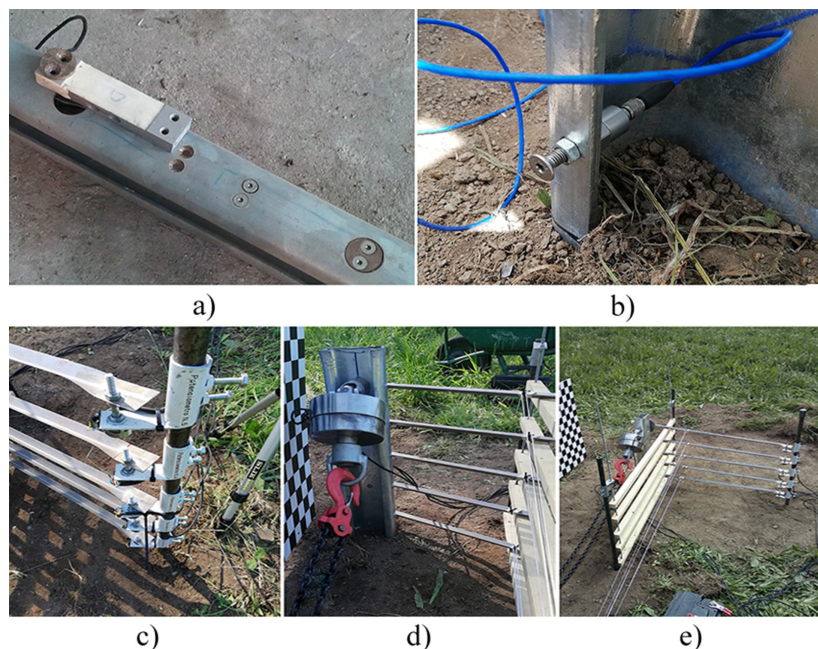


Figure 12. Field instrumentation setup: (a) load cells, (b) accelerometers, (c) potentiometers, (d) third load cell, (e) view final.

electrical resistance from zero to 1 kΩ were utilized to acquire the horizontal displacements of the guardrail post during loading, installed at 10 cm from each other, with the first at surface level (Figure 12c). Finally, a third load cell with the range of 130 kN was installed 50 cm above the surface to measure the applied horizontal loading force (Figure 12d). The final setup is shown in Figure 12e.

Regarding the test procedures, two configurations were deployed. The first one was designed as the static test configuration and consisted of loading the guardrail post at a monotonic displacement rate of 3 cm/min. To do so, two posts were driven into the ground and used for the reaction. In the dynamic test configuration (Figure 13), it was intended to apply a dynamic horizontal loading in the guardrail post, 0.5 m above the surface. To do so, a vehicle with a mass of around 1950 kg was used, moving with the speed of 15 km/h (speed component perpendicular to the guardrail post) at the time of impact. A vehicle impact with the guardrail post was supposed to happen at a narrow angle; to do that, only the component of the speed perpendicular to the guardrail post was considered.

Eight tests were defined by combining the axis of inertia, post length, and test procedure (Table 1). Figure 14 provides all the relevant geometric parameters used in the field tests.

3.2.1 Static test results

The number of potentiometers used in this study (5 in total) was later found redundant when the data was analyzed. Therefore, only the data from three potentiometers (1, 4, and 5) was considered. Potentiometer 4 was mainly used because



Figure 13. Test set-up used for the in-situ testing of the posts.

Table 1. Parameters considered for the in-situ testing of the posts.

Test ID	Mobilized axis	Length	Loading
x120s	xx	1.2 m	static
y120s	yy	1.2 m	static
x170s	xx	1.7 m	static
y170s	yy	1.7 m	static
x120d	xx	1.2 m	dynamic
y120d	yy	1.2 m	dynamic
x170d	xx	1.7 m	dynamic
y170d	yy	1.7 m	dynamic

ID: Identification.

its data was ‘cleaner’ than that collected by potentiometer 5, which was affected by some interference from the load cells.

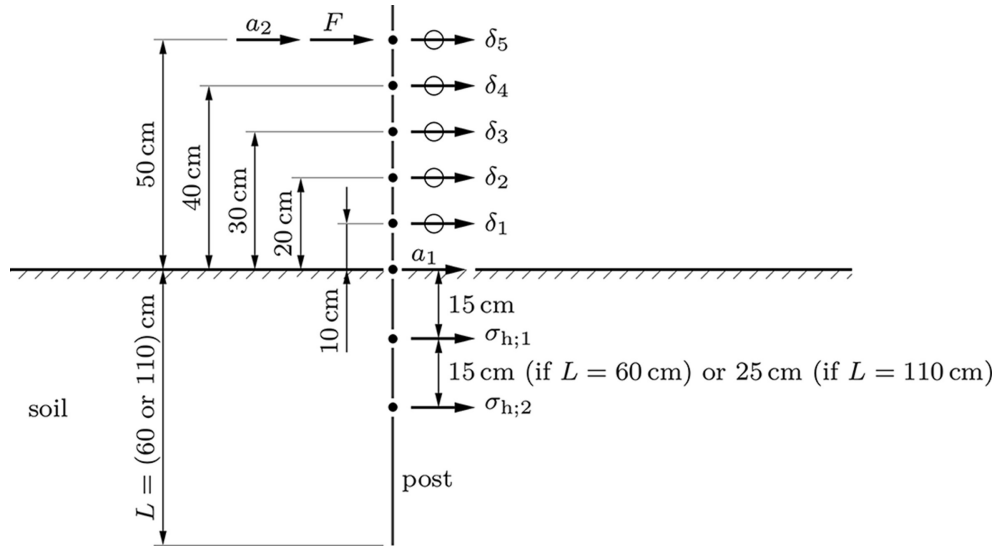


Figure 14. Geometric parameters used in all field tests (elevation view).

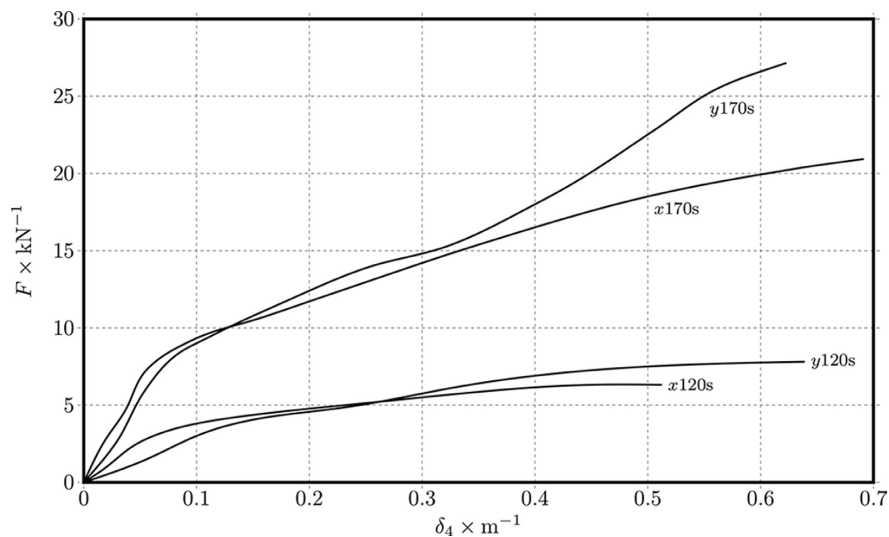


Figure 15. Static post testing - horizontal force (F) development along the imposed displacement δ_5 (represented as a function of δ_4).

The load-displacement curve presented in Figure 15 showed no peak, and the maximum static load was approximately 27 kN, at a late loading stage. The short post reached its maximum loading (7 kN) in the yy axis of inertia and the minimum loading (6 kN) in the xx axis of inertia. Similarly, the long post experienced its maximum and minimum loading in the yy axis of inertia (27 kN) and xx axis of inertia (21 kN), respectively. Regarding the imposed displacement, the short post reached its maximum displacement (0.64 m) in the yy axis and its minimum displacement (0.51 m) in the xx axis. In contrast, the long post reached its maximum displacement, of 0.69 m, around the xx axis, while the yy axis registered a lower displacement of 0.61 m. The long post absorbed a maximum loading, in the yy axis, approximately 4 times the

maximum measured loading for the short post. The long post also showed a maximum displacement, in the xx axis of inertia, higher than the maximum displacement presented by the short post in the yy axis. However, the axis of inertia was less crucial for the long post, despite experiencing an overall maximum displacement than the short post.

In terms of minimum and maximum displacements (Figure 16), at 50 cm above the ground (δ_5), the short post reached its maximum limit displacement along the yy axis of inertia, which is higher than the maximum displacement experienced by the short post around the xx axis of inertia. The long post experienced higher maximum displacements than the short post, regardless of the axis of inertia. The combined maximum limit displacement was, thus, reached by the long post.

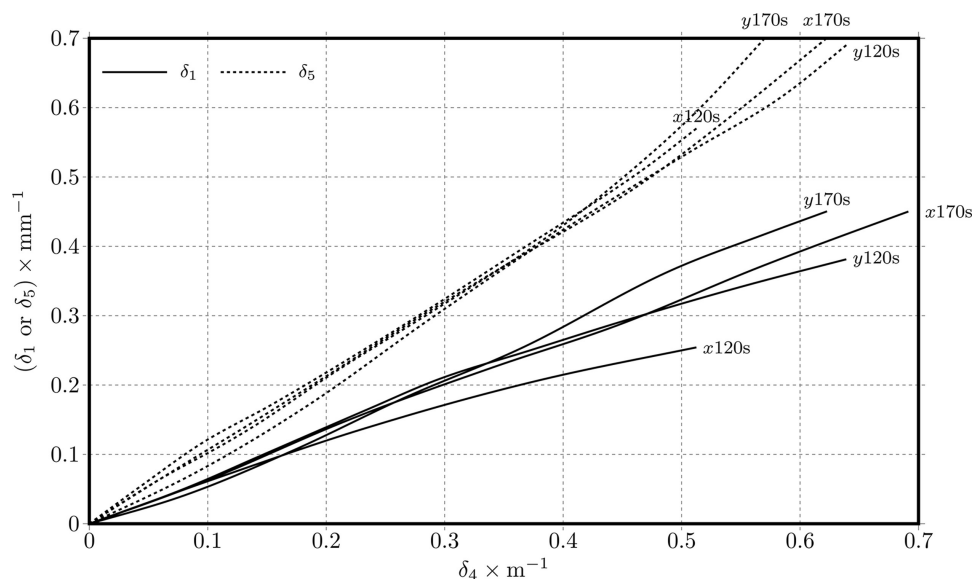


Figure 16. Static post testing - development of the minimum and maximum measured displacements (δ_1 and δ_5) as a function of the displacement δ_4 .

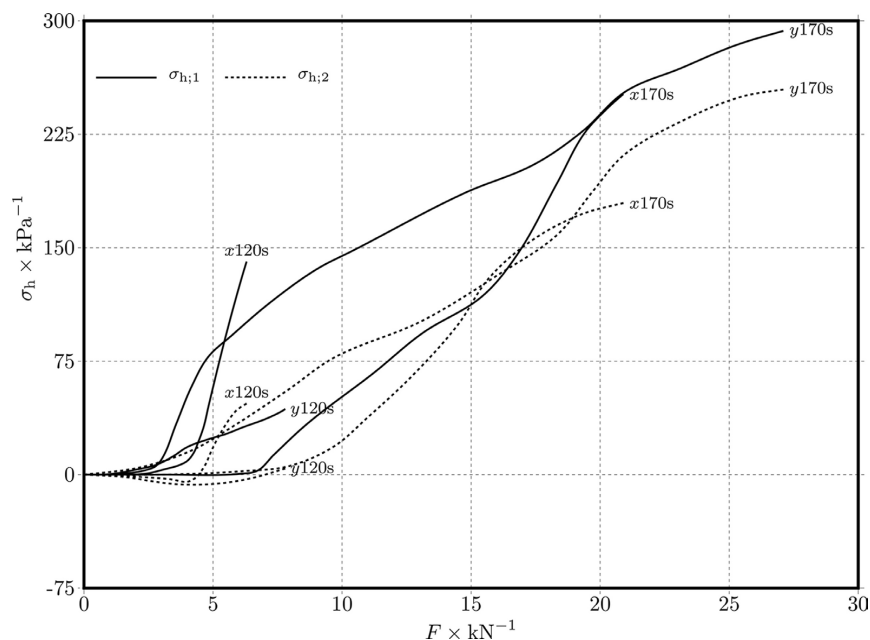


Figure 17. Static post testing - horizontal stress (σ_h) development as a function of the horizontal force (F).

At a depth of 10 cm above the ground (δ_1), the short post experienced its maximum displacement in the yy axis of inertia, while the long post showed similar displacement values for both axes of inertia. The maximum limit displacement was reached by the long post.

Regarding the horizontal stress (Figure 17), the short post in the xx axis experienced higher horizontal stress at a depth of 15 cm ($\sigma_{h,1}$) than at a depth of 30 cm ($\sigma_{h,2}$). Regarding the yy axis of inertia, the horizontal stress at 15 cm was also

higher than that at 30 cm. For the short post, the xx axis, at a depth of 15 cm, registered the maximum horizontal stress.

For the long post, the xx axis of inertia, at a depth of 25 cm, experienced higher horizontal stress than the yy axis, at a depth of 50 cm. The same situation was found regarding the 25 cm in the yy axis, which experienced higher horizontal stress than the xx axis, at 50 cm. The maximum horizontal stress registered for the long post was in the yy axis, at a depth of 25 cm.

3.2.2 Dynamic test results

During dynamic tests, accelerometers did not provide quality data due to the noise induced by the vehicle movement and belt oscillations – accelerometer a_1 provided unreadable data, and accelerometer a_2 only provided valuable data in two of the four tests performed (even if the sensor could not capture the initial response because it had a maximum range of 55 g).

Regarding the dynamic loading, the maximum dynamic peak loading was approximately 19 kN (Figure 18), reached at the middle stage of the test, in the xx axis of inertia. On the contrary, the short post experienced a higher dynamic loading (11 kN) in the yy axis of inertia. The long post absorbed a maximum loading of approximately 2 times the measured loading on the short post.

In terms of displacement (Figure 19), the short post registered a maximum value (50 cm above the surface) in the xx axis of inertia than in the yy axis. On the contrary, the long post suffered a maximum displacement in the yy axis of inertia than in the xx axis. At 50 cm above the surface, the maximum displacement was obtained by the short post in the xx axis of inertia. Regarding the minimum displacement (10 cm above the surface), the short post also showed a displacement higher in the xx axis of inertia than in the yy axis. The long post, contrary to what was observed for the maximum displacement, showed a higher minimum value in the xx axis of inertia. The displacement showed by the short post, in the xx axis of inertia, was the higher registered for 10 cm above the surface.

Regarding the acceleration spectrum (Figure 20), as expected, the long post experienced higher terminal accelerations, with higher values at both the beginning and end of the movement, as compared with the short post.

4. Numerical results

Numerical modeling in the world of geotechnical engineering is a process in which it tries to represent a real-world system through mathematical formulations that can be analyzed and computed by computational methods. In geotechnical engineering, numerical modeling is a widespread engineering technique to solve or tackle complex geotechnical subjects by computational simulation or deploying advanced equations under different geotechnical scenarios. A numerical model was created based on the results obtained from in-situ and laboratory tests. Models with optimal dimensions were created by the Plaxis 3D software to assess the behavior of guardrail posts around the two axes of inertia and different driving depths. Hardening soil constitutive model was chosen to create guardrail post models. To define the constitutive model, parameters including $E = 3.8$ MPa, $E_{ur} = 11.4$ MPa, $e_{init} = 0.779$, $v_{unsat} = 15.12$ kN/m³, $v_{sat} = 18.54$ kN/m³, $R_{inter} = 0.7$, and $\Psi = 4$ were utilized. The effect of soil suction was not considered because suction in the unsaturated zone above the phreatic level is ignored in Plaxis 3D software. Damping was not ignored (i.e., damping equal to 0) because high plastic failure is presented on the model. Due to the shallow buried depth of guardrail posts and for the sake of simplicity, it was decided to utilize constant values for the parameters of soil shown in Figure 9 during modeling.

4.1 Static model results

Guardrail posts, according to Table 1 and Figure 14, with different lengths and axis of inertia were modeled in the Plaxis 3D software. For all models created for guardrail

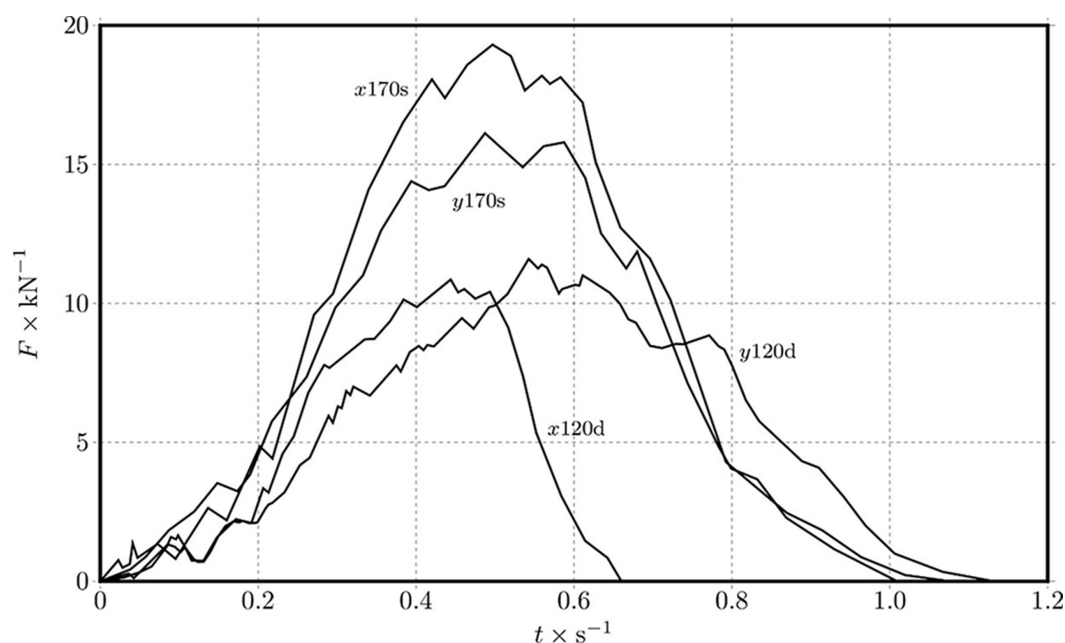


Figure 18. Dynamic post testing: horizontal force F imposed by the vehicle moving at 15 km/h.

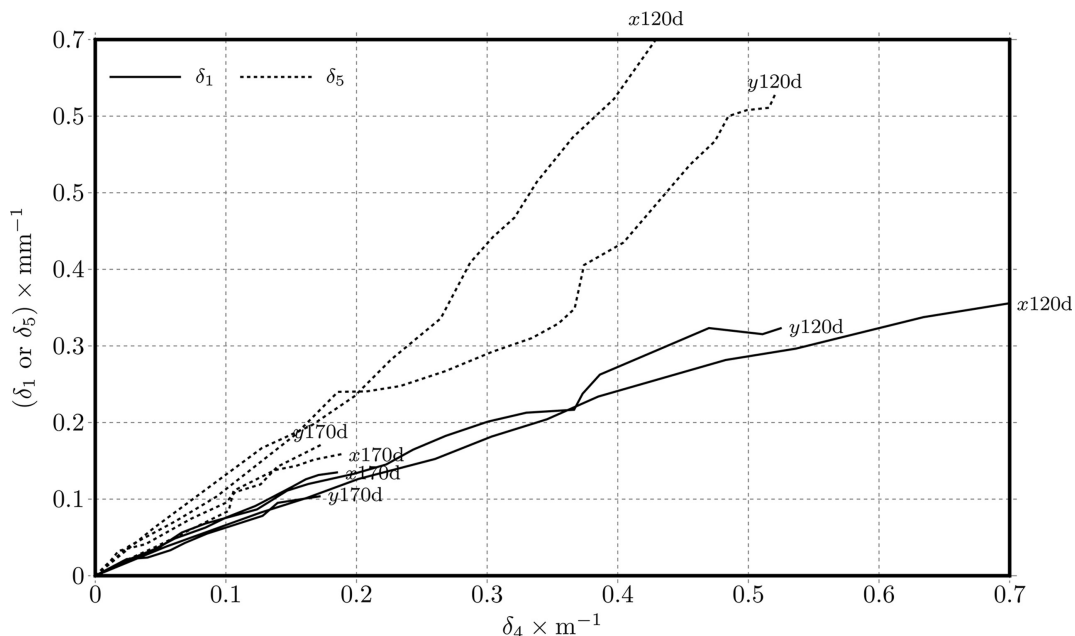


Figure 19. Dynamic post testing - development of the minimum and maximum measured displacements (δ_1 and δ_5) as a function of the displacement δ_4 .

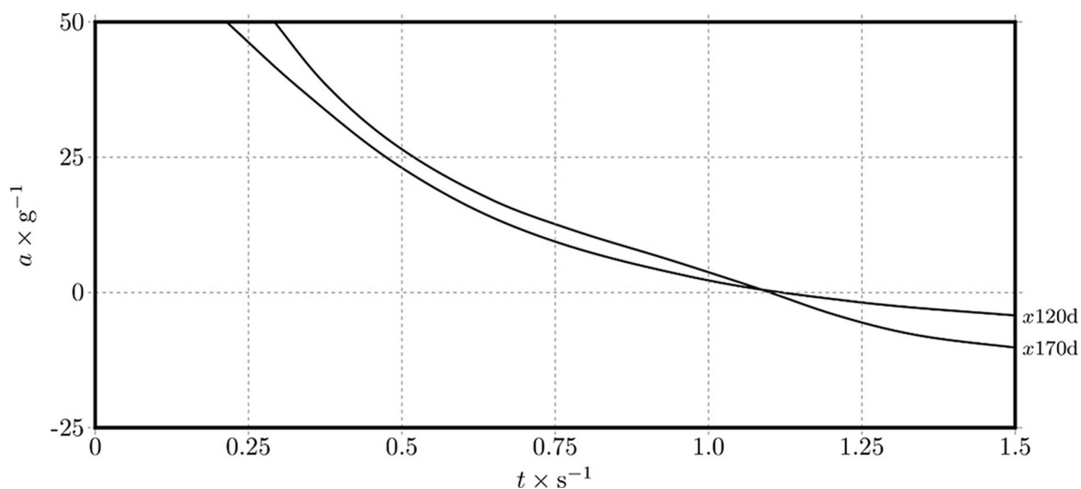


Figure 20. Dynamic post testing - acceleration spectra (time domain).

posts, loading was applied at a distance of 0.50 cm from the ground. Finally, a point displacement load proportional to the value achieved from the in-situ test was applied to models. An overview of the created model is shown in Figure 21.

After modeling guardrail posts and interpreting posts behavior, the Plaxis 3D software results indicated that numerical and experimental data are approximately equal. The final comparison to evaluate guardrail posts behavior during static loading between in-situ tests and Plaxis 3D software modeling is shown in Figure 22. Results of the comparison are based on different post lengths and axis of inertia.

4.2 Dynamic model results

Based on the in-situ results of guardrail posts behavior located on organic soil, it was decided to perform a dynamic simulation by Plaxis 3D software to validate the results between in-situ tests and Plaxis 3D models. Long posts approximately indicated equal in-situ displacement around both axis of inertia, so it was decided to just model one axis. After dynamic simulation, the results obtained in Plaxis 3D software indicated that numerical and in-situ results are almost the same, approving the accuracy of the results.

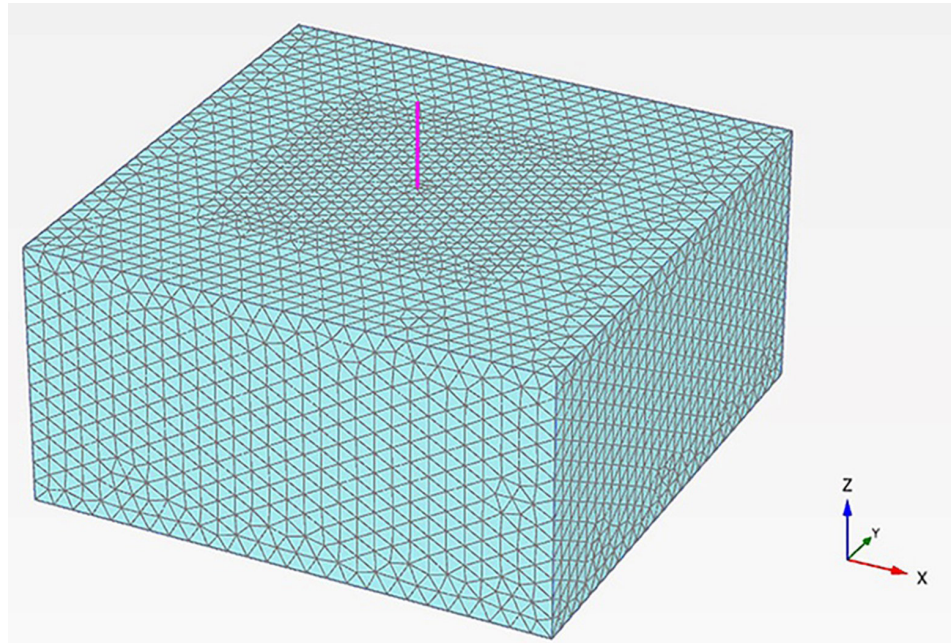


Figure 21. Guardrail post model overview.

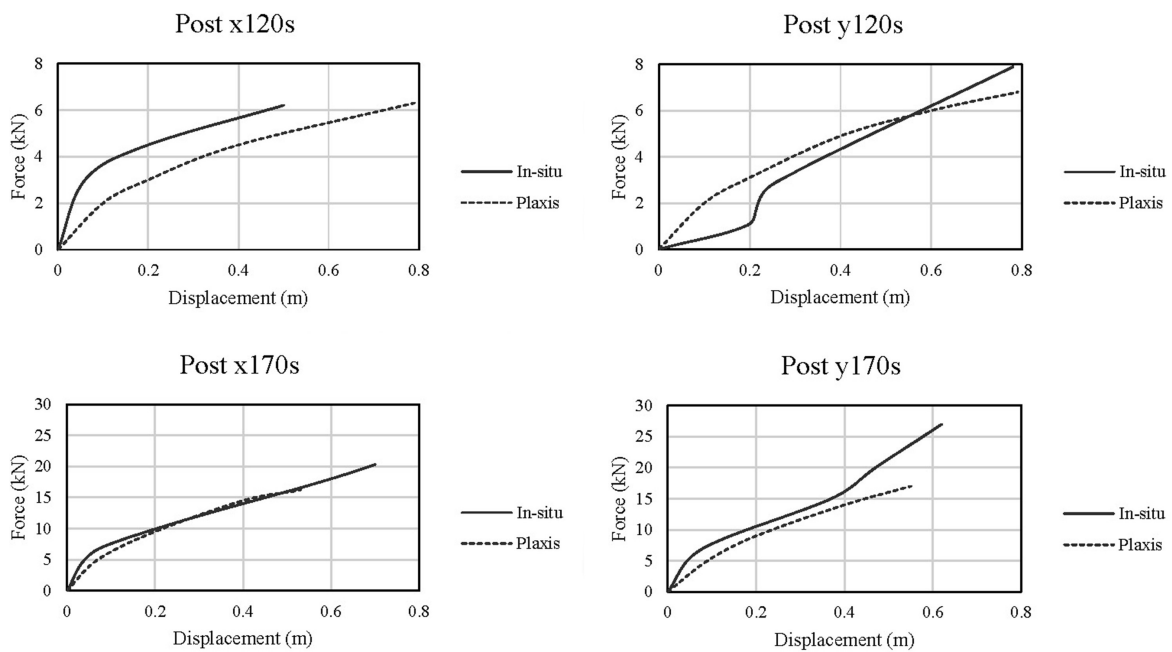


Figure 22. In-situ and Plaxis 3D results comparison in static loading.

Results of comparison based on different lengths and axis of inertia are shown in Figure 23.

5. Discussion

The dynamic and static results indicated that long guardrail posts reached maximum loading in comparison with

short posts. Besides, the short guardrail posts experienced higher minimum and maximum displacements in dynamic loading, while the long guardrail posts experienced higher minimum and maximum displacements in static loading.

From the experimental tests and results obtained, it was possible to state some critical opinions. When loading, short guardrail posts present greater deformations in the

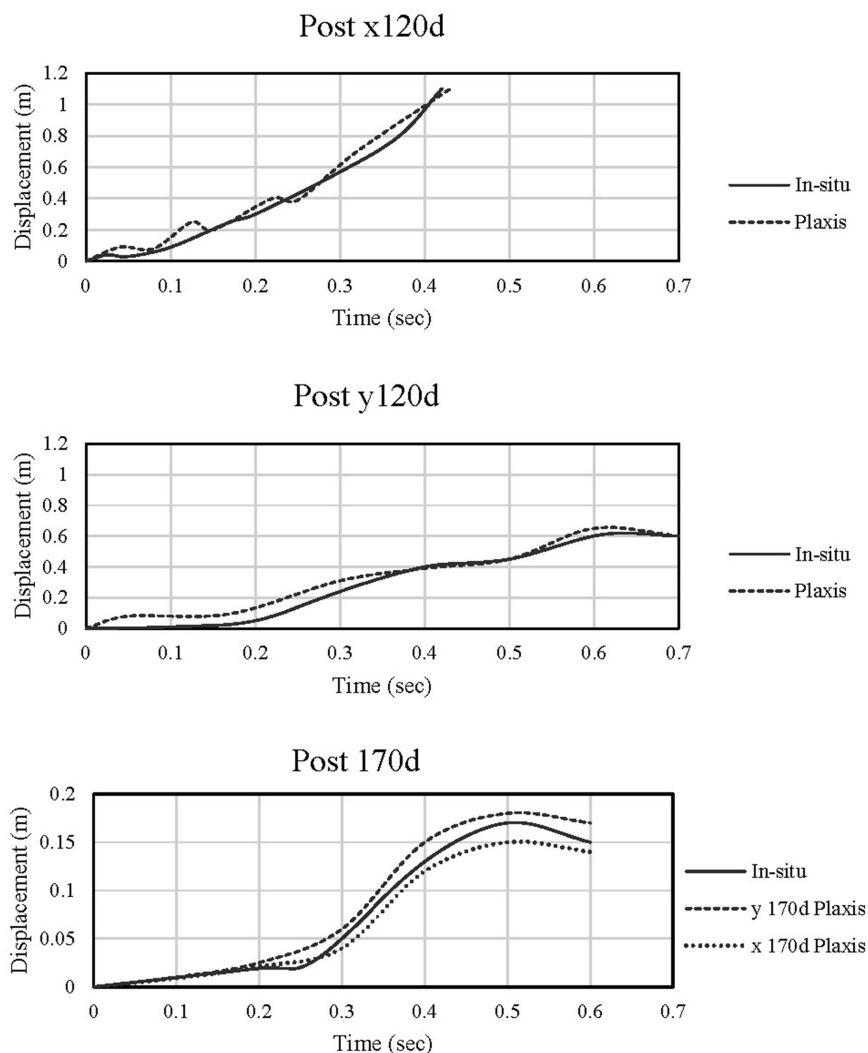


Figure 23. In-situ and Plaxis 3D results comparison in dynamic loading.

surrounding soil, while the soil under study remains stable during the loading in long guardrail posts. The guardrail posts assumed an elastic behavior due to their dimension, depth of driving, and soil strength. In addition, no relevant permanent post deformation was achieved on all tests. The guardrail post behavior turns out to be quite similar in both directions against loading.

Regarding the short guardrail posts, where the driving length was 0.6 m, it was concluded that the driving position influences the surrounding soil, both in static and dynamic tests. About long guardrail posts, where the driving length was 1.10 m, presented a much more coherent behavior due to increased driving depth. In terms of damage to the surrounding soil, the short guardrail post had a greater tendency to rotat and caused greater blistering in the surrounding soil due to the proximity of the post base on the surface. In contrast, long guardrail posts tendency to cause blistering, and tears are not evident destructively, with only occasional cracks in the soil.

6. Conclusion

This study aimed to achieve specific goals initially defined to increase knowledge of guardrail post behavior against static and dynamic loading. Despite being robust, guardrail posts start to show high ductility to protect the occupants against the impact of vehicles. After performing simplified experimental programs, it was concluded that the axis of inertia, embedment depth, and loading speed vary guardrail post behavior. Simplified numerical modeling was done to confirm the experimental results, and received data fully approved the in-situ tests. The results obtained are believed to be practical and relevant for in-situ operations and design procedures. Overall, long posts in both static and dynamic tests reached maximum loading in comparison with short posts. Short posts experienced maximum displacement in dynamic loading, while long posts experienced maximum displacement in static loading. However, it is still necessary

to provide a complete definition of the model and investigate other soil types.

Acknowledgments

The authors acknowledge the financial support by FCT / MCTES through national funds (PIDDAC) under the R&D Unit Institute for Sustainability and Innovation in Structural Engineering (ISISE), under reference UIDB/04029/2020; and ANI through national funds (Portugal 2020), under project “BARROD - Barreiras de Segurança Rodoviária”, reference 33497.

Declaration of interest

The authors have no conflicts of interest to declare. All co-authors have observed and affirmed the contents of the paper and there is no financial interest to report.

Authors' contributions

Hamid Reza Manaviparast: Conceptualization, Data curation, Visualization, Writing – original draft. Nuno Araújo: Conceptualization, Data curation, Methodology, Supervision, Validation, Funding acquisition, Project administration, Resources, Software, Writing – original draft. Nuno Cristelo: Formal Analysis, Investigation, Methodology, Tiago Miranda: Supervision, Validation, Writing – review & editing. The authors above kindly granted the permission of using parts of their publications in this template.

List of symbols

a	Acceleration
c'	Effective cohesion
c_u	Undrained cohesion
e_{init}	Initial void ratio
m	van Genuchten model parameter
n	van Genuchten model parameter
p'	Average effective stress
q	Deviatoric stress
t	Time
u	Pore water pressure
z	Depth
CD	Isotropically consolidated drained compression triaxial tests
CU	Isotropically consolidated undrained compression triaxial tests
CSL	Critical state line
D	Particle size
E	Young modulus
E_{ur}	Young modulus of unloading/reloading
F	Horizontal Force
F_y	Yield stress

K_0	Coefficient of thrust at rest
N	Vertical load
NCL	Normal compression line
OCR	Over-consolidation ratio
P	Cumulative particle size (percentage)
R^2	R-squared
R_{inter}	Reduction factor for interfaces
R_p	Soil penetration resistance
α	van Genuchten model parameter
δ	Displacement
ε_a	Axial strain
ε_v	Volumetric strain
γ_{unsat}	Unsaturated unit weight
γ_{sat}	Saturated unit weight
ϕ	Friction angle
ϕ'	Effective friction angle
ϕ_u	Undrained friction angle
ν	Poisson ratio
ρ	Volumetric weight
σ	Normal stress
σ_v	Vertical total stress
σ_h	Horizontal total stress
σ_3	Triaxial test chamber pressure
v	Specific volume
ω_s	Saturated water content
ω_r	Residual water content
ω	Water content
ψ	Soil suction
Ψ	Dilatancy angle

References

- ASTM D422-1963. (1963). *Standard Test Method for Particle-Size Analysis of Soils*. ASTM International, West Conshohocken, PA.
- ASTM D5298-94. (1994). *Standard Test Method for Measurement of Soil Potential (Suction) Using Filter Paper*. ASTM International, West Conshohocken, PA.
- Atahan, A. O., Büyük, M., Örnek, M., Erdem, M., & Turedi, Y. (2019). Determination of optimum post embedment depth for C120 steel posts using field and full scale crash test. *International Journal of Crashworthiness*, 24(5), 533-542. <https://doi.org/10.1080/13588265.2018.1479499>.
- BSI BS 1377-8. (1990). *Soil for civil engineering purposes. Shear strength test (effective stress)*. British Standards Institution, London.
- Cui, T. (2020). Research on design technology of safety facilities in highway traffic engineering. *IOP Conference Series: Earth and Environmental Science*, 587, 012006. <https://doi.org/10.1088/1755-1315/587/1/012006>.
- Gutowski, M., Palta, E., & Fang, H. (2017). Crash analysis and evaluation of vehicular impacts on W-beam guardrails placed on sloped medians using finite element simulations. *Advances in Engineering Software*, 112, 88-100. <http://dx.doi.org/10.1016/j.advengsoft.2017.04.004>.

- IGPAI NP-83. (1965). *Determinação da densidade das partículas*. IGPAI, Lisbon.
- IGPAI NP-143. (1969). *Determinação dos limites de consistência*. IGPAI, Lisbon.
- ISO ISO 22476-2:2005(E). (2005). *Geotechnical investigation and testing - Field testing - Part 2: Dynamic probing*. International Organization for Standardization, Switzerland.
- ISO ISO 22476-11:2017(E). (2017). *Geotechnical investigation and testing - Field testing - Part 11: Flat dilatometer test*. International Organization for Standardization, Switzerland.
- Jeyapalan, J.K., Dewey Junior, J.F., Hirsch, T.J., Ross Junior, H.E., & Cooner, H. (1984). Soil-foundation interaction behavior of highway guardrail posts. *Transportation Research Record: Journal of the Transportation Research Board*, (970), 37-47.
- Li, N., Park, B.B., & Lambert, J.H. (2018). Effect of guardrail on reducing fatal and severe injuries on freeways: real-world crash data analysis and performance assessment. *Journal of Transportation Safety & Security*, 10(5), 455-470. <http://dx.doi.org/10.1080/19439962.2017.1297970>.
- Lim, Y.J. (2009). Static and dynamic stability evaluation of model guardrail posts based on geotechnical properties. *International Journal of Highway Engineering*, 11(1), 233-245.
- LNEC E196. (1966). *Análise granulométrica*. LNEC, Lisbon.
- LNEC E201. (1967). *Solos. Determinação do teor em matéria orgânica*. LNEC, Lisbon.
- Mikusova, M. (2017). Crash avoidance systems and collision safety devices for vehicle occupants. In *MATEC Web of Conferences* (Vol. 107, pp. 00024). EDP Sciences. <https://doi.org/10.1051/mateconf/201710700024>.
- Neves, R.R., Fransplass, H., Langseth, M., Driemeier, L., & Alves, M. (2018). Performance of some basic types of road barriers subjected to the collision of a light vehicle. *Journal of the Brazilian Society of Mechanical Sciences and Engineering*, 40(6), 1-14. <http://dx.doi.org/10.1007/s40430-018-1201-x>.
- Örnek, M., Atahan, A.O., Turedi, Y., Erdem, M.M., & Buyuk, M. (2019). Soil based design of highway guardrail post depths using pendulum impact tests. *Acta Geotechnica Slovenica*, 16(2), 77-89. <http://dx.doi.org/10.18690/actageotechslov.16.2.77-89.2019>.
- Ozcanan, S., & Atahan, A.O. (2020). Radial basis function surrogate model-based optimization of guardrail post embedment depth in different soil conditions. *Proceedings of the Institution of Mechanical Engineers. Part D, Journal of Automobile Engineering*, 234(2-3), 739-761. <http://dx.doi.org/10.1177/0954407019848548>.
- Pajouh, M.A., Schmidt, J., Bielenberg, R.W., Reid, J.D., & Faller, R.K. (2018). Simplified Soil-Pile Interaction Modeling under Impact Loading. In S.J. Brandenberg & M.T. Manzari (Eds.), *Geotechnical Earthquake Engineering and Soil Dynamics V: Numerical Modeling and Soil Structure Interaction* (pp. 269-280). American Society of Civil Engineers.
- Patzner, G.S., Plaxico, C.A., & Ray, M.H. (1999). Effects of post and soil strength on performance of modified eccentric loader breakaway cable terminal. *Transportation Research Record: Journal of the Transportation Research Board*, 1690(1), 78-83. <http://dx.doi.org/10.3141/1690-08>.
- Rohde, J.R., Rosson, B.T., & Smith, R. (1996). Instrumentation for determination of guardrail-soil interaction. *Transportation Research Record: Journal of the Transportation Research Board*, 1528(1), 109-115. <http://dx.doi.org/10.1177/0361198196152800111>.
- Sassi, A. (2011). *Analysis of W-beam guardrail systems subjected to lateral impact*. University of Windsor.
- Tomlinson, M., & Woodward, J. (2007). *Pile design and construction practice*. CRC press. <https://doi.org/10.4324/9780203964293>.
- van Genuchten, M.T. (1980). A Closed Form Equation for Predicting the Hydraulic Conductivity of Unsaturated Soils. *Soil Science Society of America Journal*, 44(5), 892-898. <http://dx.doi.org/10.2136/sssaj1980.03615995004400050002x>.
- Yun, J.S., Han, K.J., Ahn, H., Falcon, S.S., Kim, K.D., & Choo, Y.W. (2018, June). Numerical Study on Static Behavior of Guardrail Supporting Piles Subjected to Horizontal Load. In *The 28th International Ocean and Polar Engineering Conference*. OnePetro.